Controlling the magnetic properties of $LaMnO_3$ thin films on $SrTiO_3$(100) by deposition in a O_2/Ar gas mixture

2010 J. Phys.: Condens. Matter 22 146007

(http://iopscience.iop.org/0953-8984/22/14/146007)

J. Phys.: Condens. Matter **22** (2010) 146007 (4pp) doi:10.1088/0953-8984/22/14/146007

Controlling the magnetic properties of $LaMnO_3$ thin films on $SrTiO_3(100)$ by deposition in a O_2/Ar gas mixture

H S Kim and H M Christen

Materials Science and Technology Division, Oak Ridge National Laboratory, Oak Ridge, TN 37831-6114, USA

Received 30 December 2009, in final form 8 February 2010
Published 23 March 2010
Online at stacks.iop.org/JPhysCM/22/146007

Abstract

The magnetic, structural, and transport properties of pulsed-laser deposited $LaMnO_3$ thin films are analyzed as a function of the O_2 partial pressure in the growth environment (using an O_2/Ar gas mixture). Interestingly, the magnetic properties do not change gradually as the O_2 content increases. Instead, ferromagnetism emerges rapidly with the oxygen; a critical amount of Ar is needed to suppress ferromagnetism effectively in $LaMnO_3$ thin films. The most dramatic suppression of ferromagnetism occurs only in the narrow window below 10% oxygen, where the ferromagnetic moments decrease by a factor of 17. Above a certain oxygen concentration, the ferromagnetic moment no longer increases with oxygen. The sample grown in pure oxygen shows a metal–insulator transition at ∼200 K, but exhibits an insulating behavior again below ∼150 K. This intermediate metallic behavior is significantly suppressed by using the O_2/Ar gas mixture.

(Some figures in this article are in colour only in the electronic version)

1. Introduction

$LaMnO_3$ has been studied extensively due to its interesting physical properties. Defects, doping and electronic instabilities in $LaMnO_3$ play essential roles in determining the material's properties [1–4]. Doping with divalent alkali-earth metal ions such as Ca^{2+}, Sr^{2+}, or Ba^{2+} modulates the physical properties of $LaMnO_3$ by stabilizing Mn^{3+} ions to Mn^{4+} [5, 6]. Therefore, perovskite manganites $R_{1-x}A_xMnO_3$ (where R is a rare-earth ion and A an alkaline-earth ion) have attracted much attention due to their versatile electrical and magnetic properties, including colossal magnetoresistance (CMR) and metal–insulator transitions (MIT). Even without extrinsic doping, $LaMnO_3$ has a very rich phase diagram due to its nonstoichiometry [2, 3]. Synthesis in an oxygen-rich environment yields cation vacancies rather than incorporation of interstitial oxygen [7]. The crystal structure of $LaMnO_3$ also depends on stoichiometry, varying from orthorhombic ($Pbnm$) to rhomboherally distorted cubic ($Pm3m$) to rhombohedral ($R3c$) as the oxygen content increases [3]. A cooperative Jahn–Teller (JT) distortion and orbital ordering results in type-A antiferromagnetic (AFM) order in the ground state of the stoichiometric bulk material [4]. However, even this material shows a weak magnetic moment, and it remains unclear whether this is due to spin canting or phase separation into small ferromagnetic (FM) clusters within an AFM matrix [5, 8]. Despite the tremendous amount of work on manganites, there are still many unresolved issues in the interpretation of their physical properties. In the case of thin films, studies to probe the physical phenomena are complicated by the small sample volume and the elastic strain imposed by the substrate. Recently, metallic and ferromagnetic properties have been found in heterostructure oxide material comprised of AFM insulators [9, 10]. However, the origin of these interfacial effects cannot be fully explained without first understanding the often synthesis dependent intrinsic properties of the $LaMnO_3$ films.

$LaMnO_3$ thin films are typically found to be ferromagnetic due to their nonstoichiometry [11–13]. The self-doping owing to cation vacancies causes mixed Mn valence (Mn^{3+}, Mn^{4+}) to fulfil charge neutrality. As a result, ferromagnetic double-exchange (DE) and antiferromagnetic super-exchange (SE) mechanism coexist [14]. Additional enhancement of ferromagnetism may be attributed to lattice distortions in manganites favoring a cubic crystal structure when thin films are grown on $SrTiO_3$ substrates [15]. Simultaneously, the compressive strain resulting from a $SrTiO_3$ substrate may yield FM orbital-ordered phase rather than A-type

antiferromagnetism [16]. Recently, a greatly reduced residual FM was achieved by a post-annealing [12]. However, such a post-annealing method is of limited applicability in superlattice samples. Therefore, direct control of the $LaMnO_3$ properties during the growth of thin films is required in order to explore interfacial effects within $LaMnO_3$-containing heterostructures. Here, we show that annealing is indeed not necessary, but instead the magnetic properties can be controlled by adjusting the O_2 content during film growth by pulsed-laser deposition (PLD) using an O_2/Ar mixture. Adjusting the O_2/Ar ratio at a fixed total pressure is preferred over simply varying the pressure of a pure O_2 environment, as changes in total gas pressure influence the plume dynamics, which may be accompanied by the formation of ion-impingement induced defects or stoichiometry deviations [17, 18]. In this work, the magnetic and transport properties of $LaMnO_3$ thin films on $SrTiO_3$ substrates are systematically studied for different ratios of O_2/Ar. We find that the ferromagnetism in $LaMnO_3$ is effectively suppressed only at very low O_2 concentration while T_c and transport properties vary rather gradually.

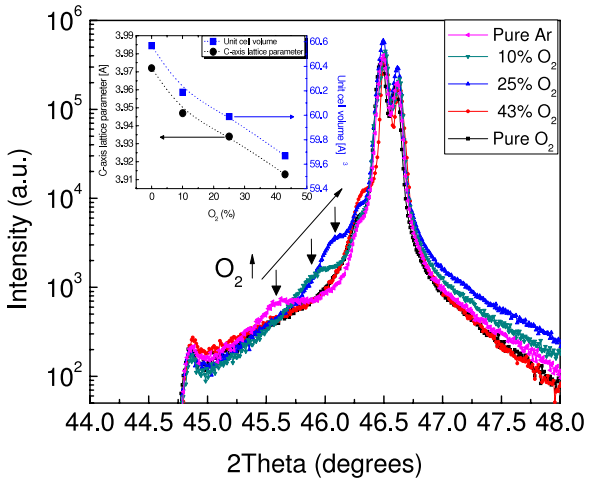

Figure 1. XRD θ–2θ scans for $LaMnO_3$ (002) films grown in a background gas with different O_2/Ar ratios. The peak splitting observed in the substrate peaks results from the polychromatic x-ray source Cu Kα_1 and Cu Kα_2 lines. The inset shows the dependence on the O_2/Ar ratio of the c-axis lattice parameter and the unit cell volume.

2. Experimental procedures

$LaMnO_3$ thin films were grown on $SrTiO_3$(100) substrates by pulsed-laser deposition. The single-crystal $SrTiO_3$ substrates were etched in buffered HF and annealed at 1100 °C for 1 h in air. A varying O_2/Ar gas mixture was used as ambient gas by varying the ratio of O_2/Ar while the growth temperature and pressure were fixed at 650 °C and 10 mTorr, respectively. Based on the system background pressure and oxygen impurities in the Ar supply, a condition of 'pure Ar' corresponds to $p(O_2) < 10^{-7}$ Torr. A commercially provided stoichiometric $LaMnO_x$ target was ablated with a KrF excimer laser (248 nm) at a fluence of ~0.4 mJ cm^{-2}. The frequency was 10 Hz, and the growth rate was 0.05 Å per laser pulse. The film thickness was about 80 nm for all samples. X-ray diffraction (Philips X'pert MRD) was used to examine the crystallinity of the films with θ–2θ scans and reciprocal space maps (RSM). The magnetic properties were characterized with a Quantum Design SQUID magnetometer. Temperature dependent transport properties were measured by a conventional four-probe method.

3. Results and discussion

3.1. Structural properties

X-ray θ–2θ scans show phase purity for all samples without any secondary phases. In order to display the data more carefully, only the 002 peaks are shown in figure 1. The films grown in <50% O_2 are clearly distinguished from the substrate and exhibit a gradual decrease of the c-axis (out-of-plane) lattice parameter with oxygen content. At larger oxygen partial pressure, the films' peaks become indistinguishable from the substrates'. As an oxygen-deficient ambient prevents the formation of Mn^{4+}, which are more abundant in an oxygen-rich condition, the decrease of the c-axis lattice parameter can be attributed to the conversion of larger Mn^{3+} ions (0.65 Å) into smaller Mn^{4+} ions (0.54 Å) [19]. The largest c-axis lattice parameter of ~3.973 Å observed in the film grown in pure Ar is accompanied by significant peak broadening for the $LaMnO_3$ 002 peak. In fact, the FWHMs (full widths at half maximum) of the film peaks increases from 0.14° for 43% O_2 to 0.25° for pure Ar. This shows that the stabilization of Mn^{3+} is accompanied by lattice disorder in the films, which is important in interpreting the magnetic and transport data, as discussed later. The inset shows the extracted c-axis lattice parameter as well as the unit cell volume. For the calculation of the unit cell volume, the in-plane lattice parameter was obtained from reciprocal space maps (RSMs) through the 114 diffraction peaks. Figures 2(a) and (b) show the RSM results for samples grown in 43% O_2 and pure Ar, respectively. The peak broadening for the latter sample makes it difficult to determine the exact peak position. However, the data obviously shows that the films are strained in-plane even at the pure Ar growth condition, i.e. $a = b = 3.908$ Å. Thus, a strong change in the lattice distortion c/a (where a is the in-plane lattice parameter, $a = 3.905$ Å) accompanies the change in unit cell volume, which must also be considered when interpreting the magnetic and transport properties. All films have a smaller unit cell volume than bulk $LaMnO_3$($V \sim 61.2$ Å^3 = [3.94 Å]^3), which may indicate that the Mn^{3+}-to-Mn^{4+} conversion occurs even at the lowest oxygen partial pressures used in this study.

3.2. Magnetic properties

The magnetization was first measured during cooling in an applied magnetic field of 2 kOe. Figure 3(a) shows the magnetic moments (per Mn ion) as a function of temperature, and figure 3(b) summarizes the phase transition temperature (T_c), defined by the inflection point in the $M(T)$ curves. The sample grown in pure Ar exhibits a transition near the bulk Neel temperature, ~140 K [2], and the magnetization versus field ($M(H)$) hysteresis loops recorded at 10 K (figure 4(a)) show a behavior consistent with weak parasitic ferromagnetism

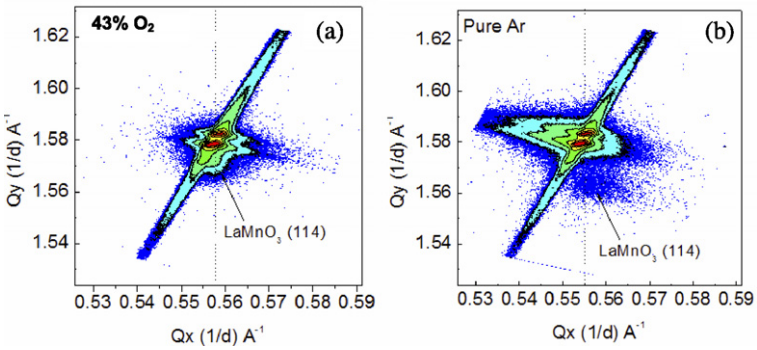

Figure 2. RSM for $LaMnO_3$ (114) grown (a) with 43% O_2 and (b) in pure Ar (b).

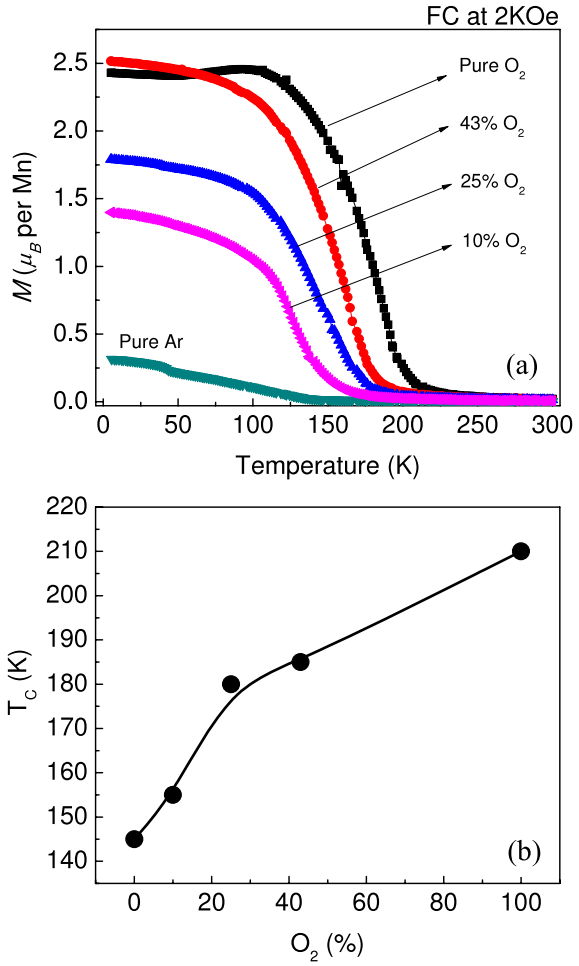

Figure 3. (a) Temperature dependent magnetization recorded during field cooling in 2 kOe, and (b) the transition temperature as a function of the O_2/Ar ratio.

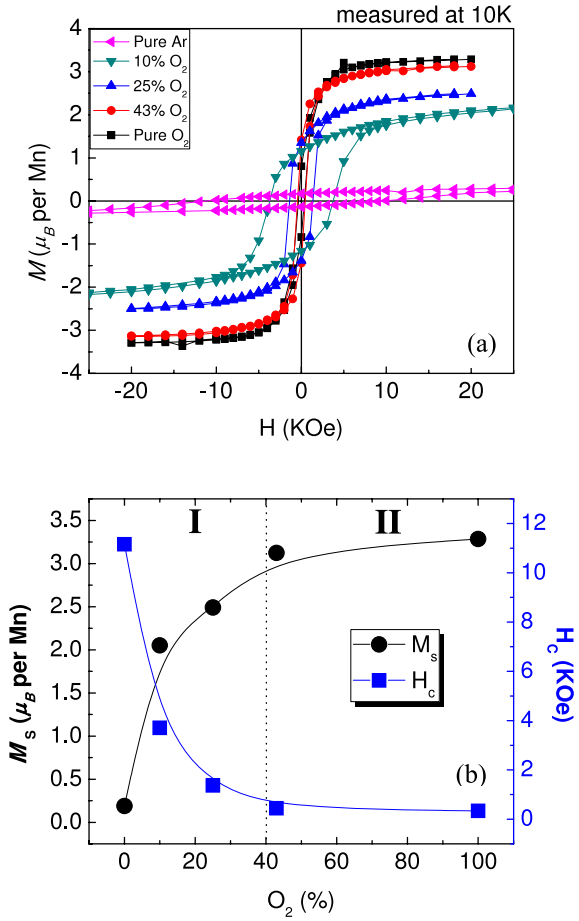

Figure 4. (a) Magnetization versus applied magnetic field at 10 K; (b) M_s and H_c as a function of the O_2/Ar ratio.

in an antiferromagnetic material. In contrast, T_c increases to 210 K for the sample grown in pure oxygen. The dominant mechanism for ferromagnetism in doped manganites is a mixed valence of Mn^{3+}/Mn^{4+}. However, structural modifications due to the presence of Mn^{4+}, lattice disorder, and strain caused by substrate must also be considered. The magnetization and transition temperature are closely related to Mn–O–Mn bond angles and Mn–O bond lengths [20–22]. A small Mn–O–Mn bond angle enlarges the Mn–O bond lengths, and thus suppresses M and T_c by reducing the e_g electron transfer integral between neighboring Mn ions [23, 24]. As mentioned before, SE and DE interactions coexist in the mixed-valent system, but the two mechanisms act on different length scales (with SE occurring at a longer bond length than DE [22]). Based on these considerations, the decrease in lattice parameter observed in this study is consistent with the increase of T_c with oxygen content. In addition, the lattice disorder observed at the lowest O_2-content may contribute to reducing M and T_c by playing a role of scattering centers.

More information is gained from analyzing the $M(H)$ curves shown in figure 4(a), indicating that M_s increases from

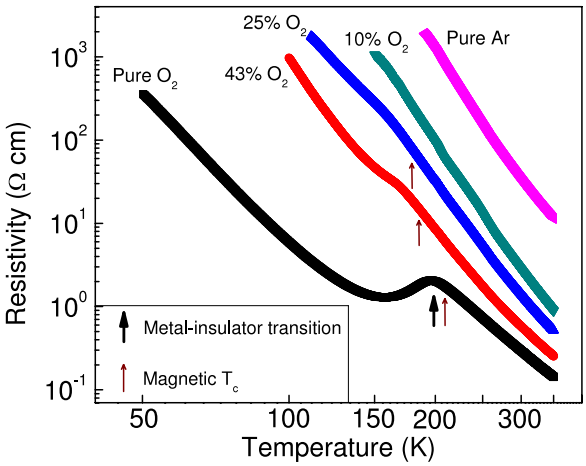

Figure 5. Temperature dependent resistivities of $LaMnO_3$ thin films grown with different O_2/Ar ratio. The bold arrows indicate a change of $\partial\rho/\partial T$. Thin arrows indicate the magnetic T_c from figure 4(b).

0.19 μ_B to 3.29 μ_B with oxygen, where M_s is defined as the y-axis intercept of the straight-line fit to the high-field (linear) portion of the data. Interestingly, this increase does not follow the same gradual change observed for T_c. In contrast, M_s rises rapidly with O_2, reaching 3.12 μ_B/Mn at 43% O_2 already, close to the value measured at pure O_2 (3.29 μ_B/Mn). This saturation near 40% O_2 may indicate a limit to the achievable level of self-doping. Conversely, a critical amount of Ar is needed to suppress ferromagnetism in $LaMnO_3$ thin films. To illustrate this behavior more precisely, M_s and H_c are plotted as a function of the O_2 concentration in figure 4(b). The range can be divided into two regions according to the sensitivity of the magnetic properties to the O_2/Ar ratio. In region I (<40% O_2), M_s and H_c are strongly dependent on the O_2/Ar ratio. In contrast, M_s and H_c do not change significantly within region II (>40% O_2) while T_c still noticeably increases with O_2. Across the entire range, M_s increases by a factor of 17, with two-thirds of the increase observed already at 10% O_2.

3.3. Transport properties

The transport properties as a function of temperature are shown in figure 5. The electrical resistivity of the $LaMnO_3$ thin films sharply decreases with O_2 concentration in the growth ambient. The sample grown in pure oxygen shows a metal–insulator (MI) transition at ∼200 K, and again insulating behavior below ∼150 K. The MI transition defined by a change of the sign of $\partial\rho/\partial T$ is indicated by bold arrows and is near the magnetic transition temperature from figure 3(a), indicated here by thin arrows. The intermediate metallic behavior just below the MI transition is observed only in films grown at the highest O_2 concentrations, and the MI transition is barely visible below 100% O_2 (showing only weak kinks near the transition temperature). Note that the resistivities for the low-O_2 samples exceed the measurement limit at low temperatures. The drastic change in transport properties across the entire range is striking in view of the small increase of M_s above ∼40% oxygen, but agrees with the gradual increase of the magnetic T_c as shown in figure 3(b).

4. Conclusion

The magnetization of $LaMnO_3$ thin films can be directly controlled by varying the oxygen partial pressure during growth with PLD, using an O_2/Ar mixture as background gas. While T_c and resistivities gradually change across the entire composition range, the magnetic moments do not follow the same gradual trend. Instead, ferromagnetism appears rapidly already at low O_2/Ar ratios. A significant suppression of ferromagnetism is observed only in the narrow region below 10% of oxygen, with M_s being reduced by a factor of 17 with respect to the 100% O_2 sample. Thus, M_s and H_c saturate at large O_2, while the resistivities and T_c change more gradually. A well-defined metal–insulator transition at ∼200 K with insulating behavior also below ∼150 K is observed in the sample grown in 100% O_2. However, the intermediate metallic behavior is rapidly suppressed by decreasing the O_2/Ar ratio.

Acknowledgment

This research was supported by the Division of Materials Science and Engineering, US Department of Energy.

References

[1] Goodenough J B 1955 *Phys. Rev.* **100** 564
[2] Ritter C, Oseroff S and Cheong S-W 1997 *Phys. Rev.* B **56** 8902
[3] Töpfer J and Goodenough J B 1997 *J. Solid State Chem.* **130** 117
[4] Salamon M B and Jaime M 2001 *Rev. Mod. Phys.* **73** 583
[5] Ramirez A P 1997 *J. Phys.: Condens. Matter.* **9** 8171
[6] Youn S J and Min B I 1997 *Phys. Rev.* B **56** 12046
[7] Subias G, Garcia J, Blasco J and Proietti M G 1998 *Phys. Rev.* B **58** 9287
[8] Skumryev V, Ott F, Coey J M D, Anane A, Renard J-P, Pinsard-Gaudart L and Revcolevschi A 1999 *Eur. Phys. J.* B **11** 401
[9] Nanda B R K and Satpathy S 2008 *Phys. Rev.* B **78** 054427
[10] Bhattacharya A, May S J, te Velthuis S G E, Warusawithana M, Zhai X, Jiang B, Zuo J-M, Fitzsimmons M R, Bader S D and Exkstein J N 2008 *Phys. Rev. Lett.* **100** 257203
[11] Murugavel P, Lee J H, Yoon J-G and Noh T W 2003 *Appl. Phys. Lett.* **82** 1908
[12] Choi W S, Marton Z, Jang S Y, Moon S J, Jeon B C, Shin J H, Seo S S A, Noh T W, Kim M-W, Lee H N and Lee Y S 2009 *J. Phys. D: Appl. Phys.* **42** 165401
[13] Gupta A, McGuire T R, Duncombe P R, Rupp M, Sun J Z, Gallagher W J and Xiao G 1995 *Appl. Phys. Lett.* **67** 3494
[14] Kleine A, Luo Y and Samwer K 2006 *Europhys. Lett.* **76** 135
[15] Dong S, Yu R, Yunoki S, Alvarez G, Liu J-M and Dagotto E 2008 *Phys. Rev.* B **78** 201102
[16] Bhattacharya A, Zhai X, Warusawithana M, Eckstein J N and Bader S D 2007 *Appl. Phys. Lett.* **90** 222503
[17] Dyer P E, Issa A and Key P H 1990 *Appl. Phys. Lett.* **57** 186
[18] Geohegan D B 1992 *Appl. Phys. Lett.* **60** 2732
[19] Shannon R D and Prewitt C T 1969 *Acta Crystallogr.* B **25** 925
[20] Liu G-L, Zhou J-S and Goodenough J B 2004 *Phys. Rev.* B **70** 224421
[21] Hwang H Y 1995 *Phys. Rev.* B **52** 15046
[22] Dutta A, Gayathri N and Ranganathan R 2003 *Phys. Rev.* B **68** 054432
[23] Fu Y 2000 *Appl. Phys. Lett.* **77** 118
[24] Malavasi L, Mozzati M C, Alessandri I, Depero L E, Azzoni C B and Flor G 2004 *J. Phys. Chem.* B **108** 13643